Dynamics of energy dissipation in heavy-ion fusion reactions

Xiang Jiang,[1] Shiwei Yan,[1,2,*] and Joachim A. Maruhn[3]
[1]*College of Nuclear Science and Technology, Beijing Normal University, Beijing 100875, China*
[2]*Beijing Radiation Center, Beijing 100875, China*
[3]*Institut für Theoretische Physik, Goethe-Universität, D-60438 Frankfurt am Main, Germany*
(Received 26 March 2013; revised manuscript received 15 August 2013; published 21 October 2013)

The dynamics of energy dissipation in head-on fusion reactions of mass-symmetric systems at low bombarding energies is studied by exploiting the improved quantum molecular dynamics model. The results indicate that the form and magnitude of the mass parameter and friction coefficient show strong dependence on system size, bombarding energy, and relative distance. The dynamical mass parameter has almost no effect on the friction coefficient. Two-body collisions play an important role in energy dissipation even when the incident energy is much lower than the Fermi energy. The nucleon-nucleon collisions not only attenuate the energy dissipation but also hinder the nucleon transfer process.

DOI: 10.1103/PhysRevC.88.044611 PACS number(s): 25.70.Jj, 24.10.−i

I. INTRODUCTION

To understand nuclear reactions, the macroscopic model plays a very important role, in which a few selected collective degrees of freedom are usually expected to contain the main information on the dynamics and are used to describe the complex dynamical process. Within such a macroscopic model, nuclear friction is a crucial ingredient introduced along the line of thought of classical friction to deal with the phenomenon that energy and angular momentum dissipate irreversibly from collective to intrinsic degrees of freedom in large-amplitude collective motion of nuclear systems, such as fusion reactions, fission, giant resonances, etc. [1–6].

The dynamics of nucleus-nucleus reactions are expected to change strongly in the energy region between $E/A = 10$ and 100 MeV. It is commonly believed that in this energy region there are two extreme mechanisms of energy dissipation in nuclear matter: one- and two-body dissipation. At low energies, due to the inhibition of nucleon-nucleon collisions by the Pauli principle which makes the nucleon-collision mean-free path comparable to or larger than the nuclear size, the one-body dissipation [7–11] is generally assumed to be the main mechanism responsible for the damping of collective motion. Above the Fermi energy ($E/A \approx 35$ MeV), nucleon-nucleon collisions are increasingly allowed, and eventually these collisions will dominate the reaction dynamics. Thus the dissipation mechanism is expected to change from mainly one-body dissipation to a mechanism governed by two-body dissipation [12–15]. Their interplay and mutual balance, however, are still a question of debate and represent a long-term controversy.

There are many theoretical approaches to the one-body dissipation problem in heavy-ion collisions (HICs). Based on phenomenological friction forces fit to the experimental data, the surface friction model (SFM) [10,16,17] and the wall-and-window formula [11,18,19] are introduced with several free parameters. The free parameters in these models, however, have no solid theoretical background. From the microscopic point of view, the friction coefficient was calculated by using time-dependent perturbation theory [7], linear response theory (LRT) [20], and the two-center shell model [21]. But the results given by these models are difficult to interpret in terms of reversible kinetic and irreversible dissipative energies. Another important and powerful tool for describing systems with long mean-free path is time-dependent Hartree-Fock (TDHF) [22,23], which is a fully microscopic quantal and self-consistent many-body theory. Unfortunately, it turns out that only the mean value can be well described by TDHF but not the fluctuations that are important for any dissipation [24,25].

There are also many different theoretical methods proposed to describe two-body dissipation, among them the Werner-Wheeler (W-W) method which is based on the assumption that the nucleus is an incompressible and nearly irrotational viscous fluid [12–14], methods based on LRT [15,26], TDHF with two-body correlations [27], etc. However, all these methods involve some strong assumptions. The uncertainty in both the strength of the nuclear friction and its form factor is still very large [28,29].

Recently, information on dissipation in the entrance channel of HICs at energies around the Coulomb barrier has been extracted by the macroscopic reduction procedure of TDHF theory, where the so-called fusion window problem due to underestimation of energy dissipation in old TDHF calculations was solved by including spin-orbit interactions and time-odd terms in the energy density functional as well as by breaking symmetries [30]. However, it is known that this study with TDHF theory still only considers a one-body dissipation mechanism from the microscopic point of view, because of the treatment of the self-consistent mean field, and an unphysical behavior of the friction coefficient exists for all the systems investigated, where the magnitude of friction coefficient rapidly decreases for decreasing relative distances within the Coulomb barrier. It seems to be worthwhile for us to perform a microscopic dynamic study of energy dissipation mechanisms which is embedded in a quantum microscopic many-body model and properly includes both one- and two-body dissipation mechanisms.

*yansw@bnu.edu.cn

In this paper, the improved quantum molecular dynamics (ImQMD) model is adopted to simulate HICs. The ImQMD model has been successfully applied to the study of HICs at both intermediate energies and at energies near the Coulomb barrier by making serious improvements [31–34]. In the model, both the nuclear mean field and the collision term allowing for nucleon-nucleon scattering, including Pauli blocking, are treated properly. Thus, in principle, the dissipation, diffusion, and correlation effects are all included without introducing any freely adjustable parameter. Using the ImQMD model, the Coulomb barriers for many reaction systems were well described [31], and the fusion excitation functions for a series of fusion reactions, including neutron-rich projectile and target reactions, were well reproduced [32]. Thus, the ImQMD model is appropriate to study the dissipation mechanism of HICs at low and intermediate energies.

The paper is organized as follows: The theoretical approach is briefly introduced in Sec. II. In Sec. III, the simulation results and detailed discussions on the dynamical nucleus-nucleus interaction potential, mass parameter, and friction coefficient are presented. In the final part of Sec. III, the relation between particle exchange and energy dissipation and the effect of two-body collisions on the dynamics of dissipation are illustrated. A summary is given in Sec. IV.

II. THEORETICAL APPROACH

The ImQMD model, like the original QMD model [35,36], is a microscopic transport model based on a molecular dynamics picture, in which each nucleon is described by a coherent state of a Gaussian wave packet singly peaked at the center of the particle. The spatial spread of the wave packet, which is an empirical parameter, is treated as system-size dependent. The total N-body wave function of the system is assumed to be a direct product of these single-particle wave packets and the one-body phase-space distribution function $f(\boldsymbol{r}, \boldsymbol{p})$ for N distinguishable particles is obtained through a Wigner transformation [37]. Then the density of the system can easily be obtained. To describe the fermionic nature of the N-body system and to improve the stability of an individual nucleus, the phase-space occupation constraint method [33] is adopted. The two-body collision correlations are introduced in a phenomenological way analogous to the test-particle calculation of the Boltzmann-Uhling-Uhlenbeck (BUU) collision term, with the interaction following [38], while Pauli blocking is handled as in Refs. [33,39].

In the ImQMD model, nucleons move in the self-consistent mean field generated by all other nucleons and the propagation satisfies the Hamiltonian canonical equations of motion on the basis of the time-dependent variational principle [40]. The Hamiltonian of the system includes the kinetic energy and effective interaction potential

$$H = T + U_{\text{eff}}, \tag{1}$$

$$T = \sum_i \frac{\mathbf{p}_i{}^2}{2m}. \tag{2}$$

The effective interaction potential includes the nuclear interaction potential and the Coulomb interaction potential,

$$U_{\text{eff}} = U_{\text{loc}} + U_{\text{Coul}}, \tag{3}$$

where U_{Coul} is written as the sum of the direct and the exchange contributions, with the latter taken into account in the Slater approximation [41],

$$U_{\text{Coul}} = \frac{e^2}{2}\int \frac{\rho_p(\mathbf{r})\rho_p(\mathbf{r}')}{|\mathbf{r}-\mathbf{r}'|}d\mathbf{r}d\mathbf{r}' - e^2\frac{3}{4}\left(\frac{3}{\pi}\right)^{1/3}\int \rho_p{}^{4/3}d\mathbf{r}, \tag{4}$$

where ρ_p is the proton density. The nuclear interaction potential reads

$$U_{\text{loc}} = \int V_{\text{loc}}[\rho]d\mathbf{r}, \tag{5}$$

where $V_{\text{loc}}[\rho]$ is the potential energy density that is obtained by the effective Skyrme interaction and is taken to be the same as that in Ref. [31]:

$$V_{\text{loc}} = \frac{\alpha}{2}\frac{\rho^2}{\rho_0} + \frac{\beta}{\gamma+1}\frac{\rho^{\gamma+1}}{\rho_0{}^{\gamma}} + \frac{g_{\text{sur}}}{2\rho_0}(\nabla\rho)^2 + g_\tau\frac{\rho^{\eta+1}}{\rho_0{}^{\eta}} + \frac{C_s}{2\rho_0}[\rho^2 - \kappa_s(\nabla\rho)^2]\delta^2, \tag{6}$$

where δ is the relative neutron excess; $\delta = (\rho_n - \rho_p)/(\rho_n + \rho_p)$. $\rho = \rho_n + \rho_p$ and ρ_n are the nucleon and neutron densities, respectively. The parameters in Eq. (6) are related to the standard Skyrme interaction parameters, with $\alpha = -356$ MeV, $\beta = 303$ MeV, $\gamma = 7/6$, $g_{\text{sur}} = 7$ MeV fm^2, $g_\tau = 12.5$ MeV, $\eta = 2/3$, $c_s = 32$ MeV, $\kappa_s = 0.08$ fm^2, and $\rho_0 = 0.165$ fm^{-3}. The corresponding incompressibility coefficient is $K_\infty = 195$ MeV.

We use the above-mentioned ImQMD model to study the dynamics of energy dissipation in head-on fusion reactions of mass-symmetric systems along the β-stability line, i.e., ^{40}Ca + ^{40}Ca, ^{64}Ni + ^{64}Ni, ^{90}Zr + ^{90}Zr, and ^{120}Sn + ^{120}Sn. Each system is investigated for two different beam energies: one near the Coulomb barrier and the other well above it.

For dynamical calculations, we first prepare the two colliding nuclei such that all the nucleons give good properties of the ground states (the binding energies and root-mean-square radii) based on the Fermi gas model. Also the nuclei should be stable without spurious emission in a sufficiently long time. After the initialization, we place the two nuclei at a separation of $3.5R_0$ on the z axis, where $R_0 = 1.16(A_P + A_T)^{1/3}$ is the radius of the compound spherical nucleus and A_P and A_T are the mass numbers of projectile and target, so that both of them are approximately in their ground states. Then they approach each other with a given bombarding energy. We generate thousands of reaction events and finally choose fusion ones from them by using the method mentioned in Ref. [42].

III. RESULTS AND DISCUSSIONS

In this work, the collective motion is studied classically while the intrinsic motion of nucleons is treated microscopically with the ImQMD model. In order to study the

collective motion with the microscopic transport model, one has to first define the collective coordinates by means of the microscopic quantities. In the QMD model, the density of the system changes dynamically and self-consistently in the whole reaction process and thus the contour plot of the density distribution of the system can be defined at each time step. An illustration of such a contour plot can be found in our previous paper [43], within which a neck position is defined at the place where densities of the projectile and target are equal. For later calculations, the portion on the right side of the neck is defined as the projectile-like fragment (PLF), and the other side is the target-like fragment (TLF).

It should be pointed out here that in the fusion process of head-on HICs, the dynamics of neck formation also plays a very important role. As discussed in Ref. [44], however, the relative and neck motions are coupled weakly and can be discussed individually. Based on this understanding, in this paper, we confine ourselves to the relative motion in head-on reactions.

With the definition of the neck position, we can easily get the collective coordinate and conjugate radial momentum of each portion for the relative motion in head-on reactions on an event-by-event basis as in Ref. [45],

$$R_i = \frac{1}{A_i}\int_{V_i} d\mathbf{r}z \int d\mathbf{p} f(\mathbf{r},\mathbf{p}), \tag{7a}$$

$$P_i = \int_{V_i} d\mathbf{r} \int d\mathbf{p} p_z f(\mathbf{r},\mathbf{p}), \tag{7b}$$

where, $f(\mathbf{r},\mathbf{p})$ is the one-body distribution function in phase space and V_i denotes the subspace with i referring to PLF and TLF, respectively. $A_i = \int_{V_i} d\mathbf{r} \int d\mathbf{p} f(\mathbf{r},\mathbf{p})$ is the mass of each subsystem. Then the mass parameter of each part is obtained as $m_i = P_i/\dot{R}_i$. $R(t) = R_{\rm PLF} - R_{\rm TLF}$ and $P(t) = (m_{\rm TLF}P_{\rm PLF} - m_{\rm PLF}P_{\rm TLF})/(m_{\rm PLF} + m_{\rm TLF})$ are the relative distance and the associated momentum, respectively. Note here that in Eq. (7) and other equations hereafter, variables are extracted on an event-by-event basis. The corresponding results presented in the figures are averaged over all fusion events through $\langle Q\rangle(x) = N_{\rm fus}^{-1}\sum_{j=1}^{N_{\rm fus}} Q_j(x)$, where $Q_j(x)$ means a specific variable value of Q for the jth fusion event and $x = t$ or R. $N_{\rm fus}$ denotes the total number of fusion events. If $x = R$, $Q_j(R) = Q_j(t_j)|_{\{t_j|R(t_j)=R\}}$ [46]. Under this definition, the nearest distance will approach $\frac{3}{4}R_0$ when the spherical nucleus forms. We should keep in mind that the method just mentioned may collapse when the overlap of the two subsystems is very large. In this case, it is unreasonable to separate the highly composite system into two parts.

The relative motion in head-on collisions can be described by one-dimensional classical equations of motion expressed as [13,47]

$$\frac{dR}{dt} = \frac{P}{\mu(R)}, \tag{8a}$$

$$\frac{dP}{dt} = -\frac{dV(R)}{dR} - \frac{d}{dR}\left(\frac{P^2}{2\mu(R)}\right) - \gamma(R)\dot{R}, \tag{8b}$$

where V is the interaction potential given later in Eq. (11), μ denotes the dynamical reduced mass, and $\gamma(R)$ is the friction coefficient.

It can be clearly seen from Eq. (8) that in the macroscopic description of the large-amplitude collective motion, the potential-energy surface, the mass parameter, and the viscosity are the most important quantities. In this section, we first show the time evolution of the relative distance $R(t)$, accompanied by the shape deformation (the mass quadrupole moment) and thermalization properties (the nuclear stopping power) of the reaction systems. Then we extract the dynamical nucleus-nucleus interaction potentials and the reduced mass parameters. In terms of the above quantities, we present the results and a detailed discussion of the system- and energy-dependent friction coefficient. In the final part, we investigate the relation between particle exchange and energy dissipation, and the role of two-body dissipation.

A. Dynamics of collective coordinates and thermalization property of reaction systems

Let us first discuss the dynamics of the collective coordinate and the thermalization property of the reaction systems. As an example, we show the time evolution of the relative distance and mass quadrupole moment of ^{90}Zr + ^{90}Zr in Fig. 1. Here the mass quadrupole moment is defined as

$$Q_{20} = \sqrt{\frac{5}{16\pi}}\int (2z^2 - x^2 - y^2) f(\mathbf{r},\mathbf{p}) d\mathbf{r}d\mathbf{p}. \tag{9}$$

In order to clearly understand such dynamical behavior, the corresponding density contour plots in the X-Z plane as well as the relative distances at some typical stages are also shown in the insets to give an impression of the reaction process. The outermost contour line corresponds to $\rho = 0.5\rho_0$.

One can see from Fig. 1 that in the head-on collisions the two colliding nuclei approach each other with the boost energy. They start to merge after they get into contact. The neck forms at the same time, and grows with increasing overlap of the two nuclei. This process is accompanied by conversion of energy from collective to intrinsic degrees of freedom. After a certain period of time, the neck disappears and the compound system is well formed. Here we should mention that medium-size systems, i.e., ^{40}Ca + ^{40}Ca, ^{64}Ni + ^{64}Ni, ^{90}Zr + ^{90}Zr, undergo a slight elongation in the direction perpendicular to the beam before the formation of the compound system, while the heavy system ^{120}Sn + ^{120}Sn, elongates in the beam direction during the whole process because of the strong Coulomb repulsion. From Fig. 1, one can also see that the reaction progress is different for the two energies at the same relative distance. The reorganization of densities in the approaching stage is more prominent when the energy is near the barrier. This effect makes neck formation take place at relatively larger distance than at higher energy. When $R = 10.65$ fm, the two nuclei begin to deform and contact each other, and a neck can be seen clearly for $E_{\rm c.m.} = 195$ MeV. At the same distance, for $E_{\rm c.m.} = 300$ MeV, however, there are two nearly spherical isolated nuclei. The deformation also reduces the barrier at lower energy, which will be shown in the following section.

It is interesting that the above results differ from those obtained by TDHF theory, in which the two-body collision effect has been neglected [48]. At energies near the Coulomb

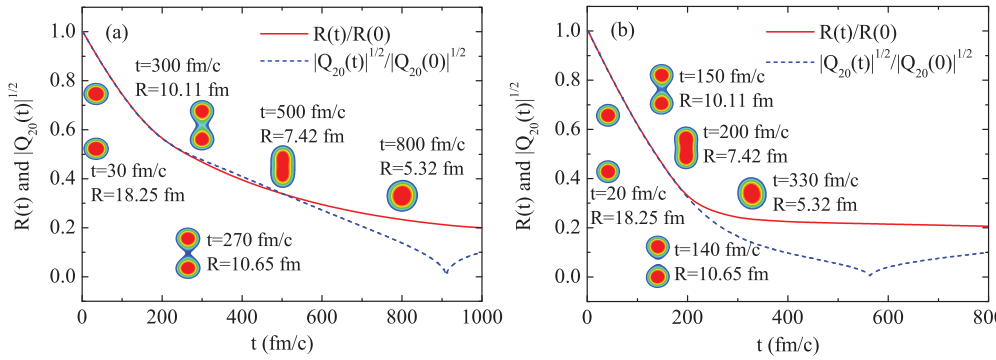

FIG. 1. (Color online) Time evolution of the relative distance and quadrupole moment scaled by their initial values for ^{90}Zr + ^{90}Zr. The data are for head-on collisions and for two different incident energies (a) $E_{\text{c.m.}} = 195$ MeV and (b) $E_{\text{c.m.}} = 300$ MeV. As an illustration, the density contour plots of some typical stages are given.

barrier, the TDHF results have shown a collective vibration behavior. The two ions may penetrate each other and bounce back under the repulsive force. Then they approach again when the attractive force offsets the repulsive force and stops the relative motion. The system thus flows into collective vibrations. The fusion process is much longer than in the ImQMD model where the nucleon-nucleon correlations are included. This difference indicates that two-body collisions may play an important role in the dynamics of fusion reactions. The role of two-body collisions in the energy dissipation process will be discussed further in the following Sec. III E.

To see the dynamical process clearly we also calculate the isotropy ratio R_p in momentum space which reflects the thermalization property and nuclear stopping of the composite system and is expressed as [50]

$$R_p = \frac{2}{\pi}\frac{\Sigma p_\perp(i)}{\Sigma p_z(i)}, \tag{10}$$

where $p_\perp(i) = [{p_x}^2(i) + {p_y}^2(i)]^{1/2}$ and $p_z(i) = [{p_z}^2(i)]^{1/2}$, the indices x, y, z stand for the three Cartesian components of momentum of the ith particle, and the sum is over all particles in the composite system. The results of R_p are shown in Fig. 2. The arrows stand for the time when the Coulomb barrier is reached. When the incident energy is around the barrier, the change of R_p is not drastic compared with higher energy,

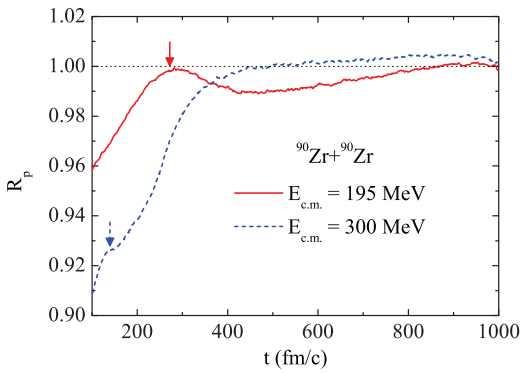

FIG. 2. (Color online) Time evolution of the nuclear stopping power of ^{90}Zr + ^{90}Zr. The center-of-mass energies are the same as in Fig. 1.

because at low energy most of the momentum is associated with Fermi motion. From the figure one can see that the linear momentum in the z direction does convert into the x and y directions because of Coulomb repulsion in the approaching stage. After they come across the barrier, the inverse process happens because of the nuclear attraction effect. After reaching a minimum, R_p rises again with the increase of the overlap and the more violent nucleon collisions. We should notice that $R_p > 1$ indicates a preponderance of momentum flow in the direction perpendicular to the beam, while $R_p < 1$ is characteristic of partial transparency [50]. This result shows the same properties as in Fig. 1. The equilibration process takes much more time if the energy is close to the barrier.

B. Dynamical nucleus-nucleus interaction potential

In order to evaluate Eq. (8) and obtain the friction coefficient, we have to calculate in advance the dynamical nucleus-nucleus interaction potential and the mass parameter of relative motion. The nucleus-nucleus interaction potential is very important for interpreting the fusion cross sections because it determines the fusion path and the mechanism of fusion. From the experimental point of view, the fusion barrier distributions can be obtained directly from the measured fusion excitation functions, with which information on the nucleus-nucleus potential around the fusion barrier can be obtained. In theory, the obtained barrier heights with different models are close to one another and all of them are comparable to the extracted mean barrier height, while the calculated nucleus-nucleus potentials at short distances strongly depend on the models and methods.

By using the ImQMD model, we can calculate the dynamical nucleus-nucleus interaction potential in fusion reactions even at short distance [43], because in the ImQMD model, the position and momentum of each nucleon can be followed at every time step. In our calculations, the nucleus-nucleus potential is described self-consistently in a way like the entrance channel potential [51],

$$V(R) = E(\rho_{\text{PLF}} + \rho_{\text{TLF}}) - E(\rho_{\text{PLF}}) - E(\rho_{\text{TLF}}), \tag{11}$$

where $E(\rho)$ is the integral of the time-dependent energy-density functional corresponding to Eq. (1), in which the kinetic-energy density functional is described by the extended Thomas-Fermi (ETF) method [52] in order to remove the contribution of collective motion.

In our previous paper [43], we applied the ImQMD model to study the dynamical barrier of heavier and asymmetric reaction systems. We concluded that the dynamical barrier encountered in the fusion process strongly depends on the incident energy. Its height decreases with decreasing incident energy and finally approaches a value which is close to the adiabatic barrier calculated by Strutinsky's macroscopic-microscopic method. With increasing incident energy the dynamic barrier increases and approaches the result calculated with the frozen-density approximation.

Following the procedure proposed in our previous paper [43], we extracted the dynamical interaction potentials of the lighter and symmetric reaction systems, as shown in Fig. 3. For comparison, we also show the results of TDHF for the ^{40}Ca + ^{40}Ca system [49] and the Bass nucleus-nucleus potential [53] for each system. The barrier positions (R_B) are labeled by arrows. We can clearly find the same trend as shown in Ref. [43]. One can see that both the Coulomb barrier and its position depend on incident energy. The barriers increase while the barrier positions decrease with increasing bombarding energies. The dynamical potentials are different from the Bass ones, especially for the incident energies around the barriers and for heavier systems (except for ^{120}Sn + ^{120}Sn around the barrier). This means that the reorganization of densities due to the strong mean field should be taken into account. It is intriguing that the dynamical potential and barrier height obtained in this paper are comparable to the results of the TDHF calculations [54].

C. Dynamics of mass parameter of relative motion

We now study the dynamical mass parameters according to Eq. (8a). Figure 4 shows $\mu(R)/\mu_0$ as a function of the scaled relative distance for two different energies. $\mu_0 = mA_PA_T/(A_P + A_T)$ is the static reduced mass when both of the two nuclei are in their ground states, where m is the nucleon mass. The fluctuations, especially for the case of energies around the Coulomb barrier, are mainly due to a small number of fusion events simulated by the ImQMD model. They do not, however, prevent an understanding of the underlying physics.

From Fig. 4, it can be seen that the mass parameters show a universal strong dependence on the relative distance, the size of the reaction system, and the incident energy. In the approaching configuration ($R \gg R_B$), $\mu(R) \approx \mu_0$. As the two colliding nuclei get closer, $\mu(R)$ increases as a function of the relative distance. The system-size and energy dependence of $\mu(R)$ can be seen from the steepness of this increase with respect to R. For the heavier system and/or higher energy, a steeper slope is observed at smaller relative distance.

The mass parameters finally reach values between 1.01 to 1.3 times μ_0 when $R = 0.9R_0$ in the given range of incident energies. Note that the above-mentioned results are comparable with those obtained by other models, such as TDHF theory [54].

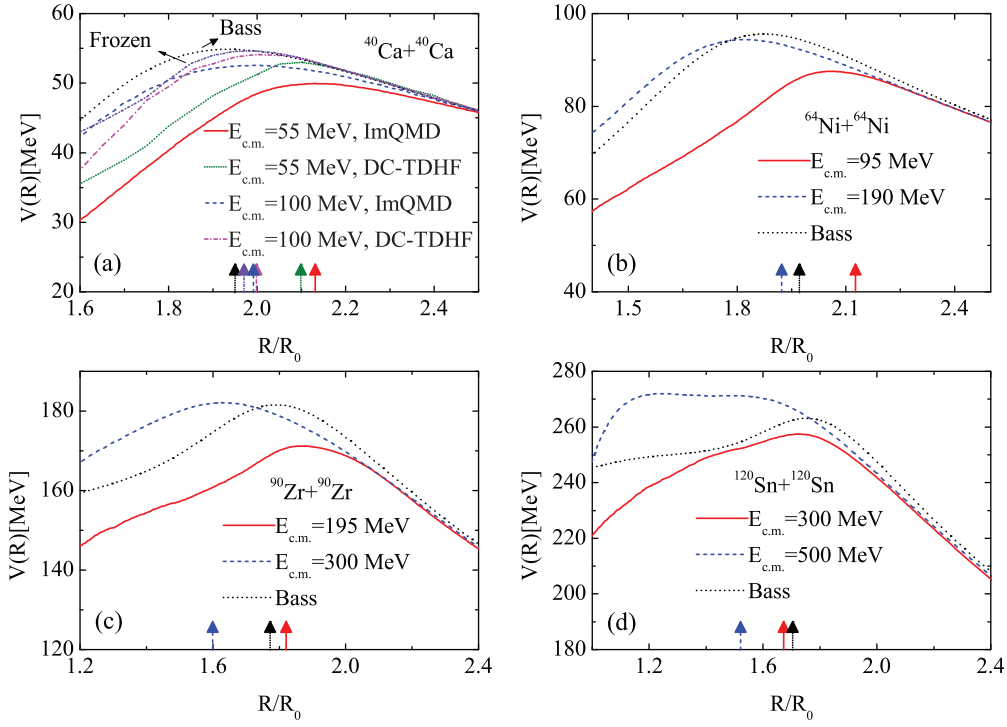

FIG. 3. (Color online) Dynamic interaction potentials of the four systems. Each system is investigated under two different energies (see text). The Bass interaction potentials and DC-TDHF results [49] are given for comparison. The corresponding barrier positions are labeled by arrows.

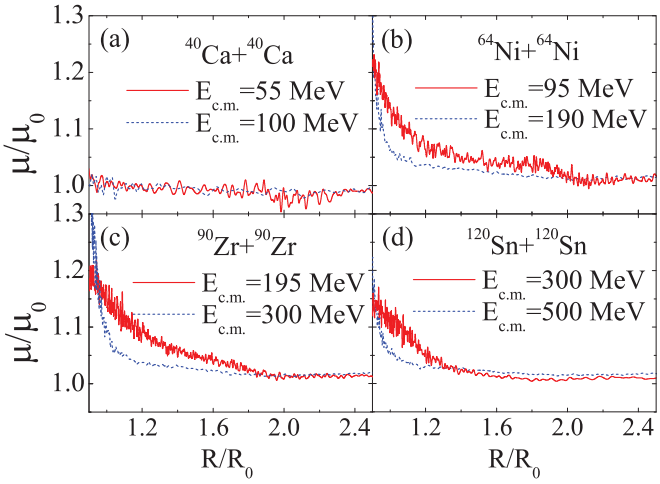

FIG. 4. (Color online) Dynamic reduced mass parameters of the four different systems as functions of the internuclear distance divided by R_0. Each system is investigated at two different beam energies. The solid and dashed lines are related to lower and higher center-of-mass energies, respectively.

D. Dynamics of friction coefficient

We are now in a position to investigate the friction coefficient based on the above results for the dynamical nucleus-nucleus interaction potential and mass parameter of relative motion, which is regarded as a main purpose of this paper.

We focus on the reduced friction coefficient, which is defined as $\beta(R) = \gamma(R)/\mu(R)$, for the reaction systems ^{40}Ca + ^{40}Ca, ^{64}Ni + ^{64}Ni, ^{90}Zr + ^{90}Zr, and ^{120}Sn + ^{120}Sn for different energies, where $\mu(R)$ and $\gamma(R)$ are derived from Eq. (8). In Fig. 5 we show $\beta(R)$ for the same systems and energies as in Fig. 4 as a function of the scaled relative distance. One can see from Fig. 5 that the friction coefficient shows a strong dependence on the relative distance, the incident energy,

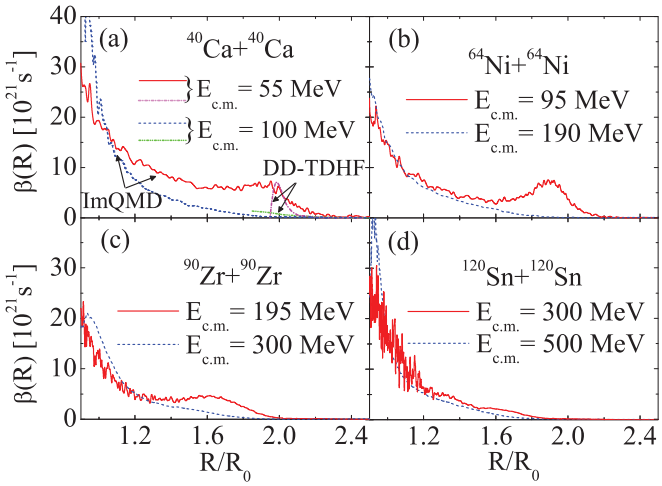

FIG. 5. (Color online) Friction coefficient for the same systems and energies as in Fig. 4. The solid and dashed lines are related to lower and higher center-of-mass energies, respectively. The results of DD-TDHF are taken from Ref. [30].

and the size of the reaction system. This property is similar to the dynamical mass parameter shown in Fig. 4. When the two colliding nuclei are far apart, $\beta(R)$ is almost 0, which is in accordance with $\mu(R) \approx \mu_0$ in Fig. 4 where both projectile and target are almost in their ground states. Then $\beta(R)$ increases with decreasing relative distance, but the form factor depends strongly on the bombarding energy. When the center-of-mass energy is much higher than the Coulomb barrier, the reduced friction coefficient increases monotonically and the trend is almost independent of the reaction system. This result is in accordance with that reported in Refs. [26,30,55,56]. When the incident energy is around the Coulomb barrier, the behavior of $\beta(R)$ becomes complicated after the touching configuration. From Fig. 5, one can see that there is a peak around the barrier position R_B for all systems investigated here (except for ^{120}Sn + ^{120}Sn, as the lower incident energy of this system is higher than the Coulomb barrier due to "extra-push" energy for fusion). This enhanced dissipation around the Coulomb barrier energies is partly due to early neck formation accompanied by an increase of nucleon exchange between projectile-like and target-like nuclei and long mean-free path of the nucleons. The magnitude of the peaks is about 8×10^{21} s^{-1}, which is identical with that of dissipative dynamics TDHF (DD-TDHF) [30]. With the increase of the incident energy, the peak moves toward smaller relative distance and the maximum decreases until it vanishes. Finally, $\beta(R)$ reaches a magnitude of 20 to 40×10^{21} s^{-1}, which is in the range of those given in Refs. [13,55,57].

In particular, we compare the results of the system ^{40}Ca + ^{40}Ca with those obtained by DD-TDHF [30]. The trends are almost the same when $R > 2.0R_0$, which indicates that the mean field may play a dominant role in energy dissipation before reaching this distance. After that, the pure mean-field theory gives unphysical results [30], which gives another evidence that two-body collisions are important in energy dissipation. A detailed study of the role of the two-body collisions in the dissipation process of fusion reactions will be given in the following section.

We also studied the effect of the dynamical mass parameter on the friction coefficient. In Fig. 6, as an example, this is presented for ^{64}Ni + ^{64}Ni. Similar results are obtained for

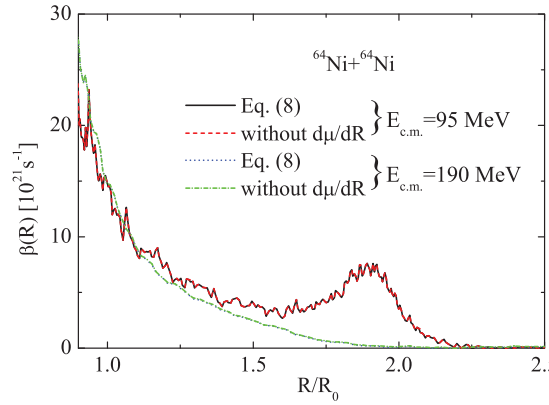

FIG. 6. (Color online) Friction coefficients for ^{64}Ni + ^{64}Ni reactions obtained with and without the second term on the rhs of Eq. (8b) at two different energies.

other reaction systems. The solid and dashed lines are the results for $E_{\text{c.m.}} = 95$ MeV while the dash-dotted and short dash-dotted lines refer to $E_{\text{c.m.}} = 190$ MeV. The solid and dash-dotted lines indicate results with the second term for $\mu(R)$ in the right-hand side (rhs) of Eq. (8b) included, while the dashed and dotted lines correspond to the results neglecting this term. We find that this term almost does not affect the friction coefficient in the whole process, although $\mu(R)$ shows a strong dependence on the relative distance and incident energy. So in practical simulations the second term on the rhs of Eq. (8b) could be neglected without causing any physical problems.

E. Effect of particle exchange and two-body collisions on dissipation dynamics

Particle and mass exchange are very important in HICs and are associated with the energy dissipation. It is well known that the nucleon transfer from projectile to target and vice versa is the main reason for energy dissipation in HICs. In this section, we illustrate the relation between particle exchange and energy dissipation. The number of nucleons transferred through the neck from target to projectile is estimated by

$$N_{\text{trans}} = \sum_{i=1}^{A_T} \int_{Z_{\text{neck}}}^{\infty} \rho_i(\mathbf{r}) d\mathbf{r}, \tag{12}$$

where $\rho_i(\mathbf{r})$ is the density distribution of the ith particle. The result is the same for the inverse process in mass-symmetric systems.

We can extract the dissipated energy from energy conservation as follows:

$$E_{\text{diss}}(R) = E_{\text{c.m.}} - \frac{P^2}{2\mu(R)} - V(R), \tag{13}$$

where the second term is the kinetic energy of relative motion. Note here that the kinetic energy of the neck is considered as a part of the intrinsic excitation energy. $V(R)$ is obtained from Eq. (11).

We take $^{40}\text{Ca} + ^{40}\text{Ca}$ as an example to see the relation of particle exchange and energy dissipation at two different incident energies, and to study the role of two-body collisions in energy dissipation. First we give the results of particle exchange and dissipated energies in the left panels of Fig. 7. The results are qualitatively the same for the two different energies. From Fig. 7(a), however, one can see that there are more nucleons transferred at lower energy compared to the case of higher energy at the same distance. This is caused by the density reorganization and neck formation which could be seen clearly in Fig. 1. One can also see that both the number of transferred nucleons and the amount of dissipated energy increase with decreasing relative distance. This indicates that energy dissipation in the early stage of the fusion reactions is strongly correlated to the nucleon transfer process.

In order to see the effect of two-body collisions, we carry out simulations on relative distance, quadrupole moments, and the isotropy ratio in momentum space, and find out that without two-body collisions, the results are similar to TDHF theory; namely, the two nuclei will bounce back after

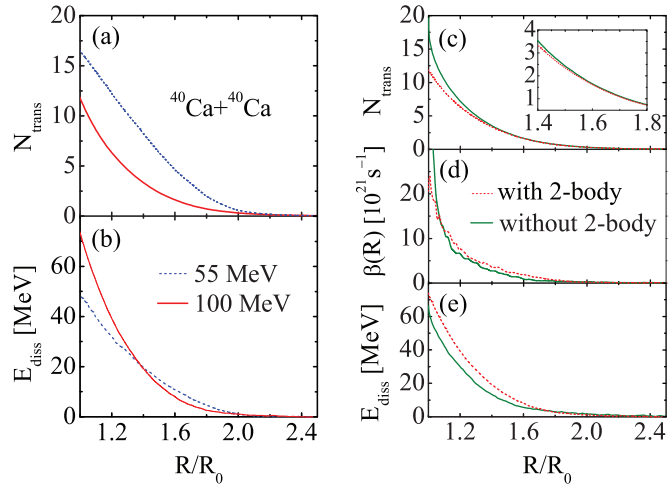

FIG. 7. (Color online) (left panels) Relative distance dependence of the nucleons transferred and energies dissipated at two different energies, and (right panels) the effect of two-body collisions in nucleon transfer and energy dissipation at $E_{\text{c.m.}} = 100$ MeV of $^{40}\text{Ca} + ^{40}\text{Ca}$.

a specific distance is reached and the system flows into collective vibrations before the compound nucleus forms. In particular, we compare the results for the number of transferred particles, the friction coefficient, and the dissipated energy by using the ImQMD model with and without two-body collisions. The results are presented in the right panels of Fig. 7 as a function of the scaled internuclear distance; the panels from top to bottom show transferred nucleons, friction coefficients, and dissipated energies, respectively. The transfer of nucleons is unaffected by collisions down to a distance of about $1.4R_0$ and then it is reduced because particles can be deflected before or during their traversal of the neck. This should lead to a reduction of one-body dissipation according to the wall-and-window formula. In contrast, the dissipated energy with two-body collisions gives larger values than that without two-body collisions at all R. The friction coefficient of two-body collisions is larger at $R > 1.1R_0$ and smaller at $R < 1.1R_0$. Since it multiplies the relative velocity $\dot{R}$ in Eq. (8b), which goes to zero at the turning point, this might not be significant.

The separation of the effects of one-body and collisional dissipation is not trivial. The case of one-body dissipation is well defined, as it requires only the absence of two-body collisions. If two-body collisions are added, however, it cannot be said that the dissipation is a sum of two separate contributions. Instead, the total dissipation arises from an interplay of these two effects; if classical transport theory can be used as a guidance, the two-body collisions are responsible for the establishment of local equilibrium and the one-body dissipation is related with transport of momentum (viscosity) and energy (thermoconductivity) with coefficients proportional to the mean-free path. In a recent paper on the Wigner function in TDHF [58] it was also found that one-body dissipation does not suffice to reach thermal equilibrium. While the reduction of the mean-free path, which is clearly visible in the decreased nucleon transfer, should reduce the

contribution of the one-body dissipation, it is not possible to separate which part of relative slowing down is due to exchanging particles through the neck (window formula), reflection from the moving potential wall (wall formula), or randomization by direct collisions, at least not on the basis of a macroscopic analysis as set up in Eqs. (8a) and (8b).

IV. SUMMARY

We have investigated the dynamics of energy dissipation in head-on fusion reactions of mass-symmetric systems along the β-stability line and at low bombarding energies by using the ImQMD model in which both the mean field and two-body collisions are taken into account. The motion of the single particles inside the nuclei is studied microscopically under the self-consistent mean field combined with nucleon-nucleon collisions while the collective motion is classically treated by a set of one-dimensional macroscopic transport equations.

The dynamics of the relative motion and nuclear stopping power of the reactions indicate that the density reorganization and neck formation take place at relative larger distance for beam energies around the barrier and that the system will be elongated in the direction perpendicular to the beam before the final compound nucleus forms. We extract dynamical interaction potentials, which suggest that the barriers depend strongly on the size of the systems and the incident energies. Crucial attention is paid to the dynamics of the mass parameter and friction coefficient. The results show that the reduced mass parameter has almost the same behavior as the friction coefficient. The form and magnitude of both show a strong universal dependence on the relative distance and incident energy. Nevertheless, the dynamical mass parameter has very little effect on the evolution of the friction coefficient. When the incident energy is much higher than the Coulomb barrier, the reduced friction coefficient increases monotonically with decreasing relative distance, and the magnitude is $20 \sim 40 \times 10^{21}$ s^{-1} at short distance, which is in satisfactory agreement with other models. The behavior becomes complicated, however, when the incident energy is close to the barrier. There is a peak with a magnitude of 8×10^{21} s^{-1}. Both the number of transferred nucleons and the amount of dissipated energy increase as a function of the relative distance, which indicates that the energy dissipation is strongly associated with the particle exchange process.

ACKNOWLEDGMENTS

One of the authors (X.J.) thanks Professor Fumihiko Sakata for helpful discussions. The authors thank the referee for pertinent suggestions that greatly contributed to improve the original manuscript. This work is partly supported by the National Nature Science Foundation of China under Grant No. 10975019, the Foundation of the Ministry of Personnel of China for Returned Scholars under Grant No. MOP2006138, and the Fundamental Research Funds for the Central Universities as well as by the German Ministry BMBF under Grants No. 06FY9086 and No. 05P12RFFTG. The numerical simulation is supported by the HSCC of Beijing Normal University.

[1] H. Steinwedel, J. H. D. Jensen, and P. Jensen, Phys. Rev. **79**, 1019 (1950).
[2] J. Bondorf, M. Sobel, and D. Sperber, Phys. Rep. **15**, 83 (1974).
[3] P. Fröbrich, Phys. Rep. **116**, 337 (1984).
[4] P. Grang and H. Weidenmüller, Phys. Lett. B **96**, 26 (1980).
[5] G. Chaudhuri and S. Pal, Phys. Rev. C **63**, 064603 (2001).
[6] R. W. Hasse, Rep. Prog. Phys. **41**, 1027 (1978).
[7] R. Beck and D. Gross, Phys. Lett. B **47**, 143 (1973).
[8] D. Glas and U. Mosel, Phys. Lett. B **49**, 301 (1974).
[9] J. R. Birkelund, J. R. Huizenga, J. N. De, and D. Sperber, Phys. Rev. Lett. **40**, 1123 (1978).
[10] D. Gross, Nucl. Phys. A **240**, 472 (1975).
[11] A. J. Sierk and J. R. Nix, Phys. Rev. C **21**, 982 (1980).
[12] J. Schirmer, S. Knaak, and G. Süssmann, Nucl. Phys. A **199**, 31 (1973).
[13] K. T. R. Davies, A. J. Sierk, and J. R. Nix, Phys. Rev. C **13**, 2385 (1976).
[14] J. R. Nix and A. J. Sierk, Phys. Scr. **10**, 94 (1974).
[15] S. Pal and N. Ganguly, Nucl. Phys. A **370**, 175 (1981).
[16] D. Gross and H. Kalinowski, Phys. Lett. B **48**, 302 (1974).
[17] D. Gross and H. Kalinowski, Phys. Rep. **45**, 175 (1978).
[18] J. Blocki, Y. Boneh, J. Nix, J. Randrup, M. Robel, A. Sierk, and W. Swiatecki, Ann. Phys. (NY) **113**, 330 (1978).
[19] J. Randrup and W. Swiatecki, Ann. Phys. (NY) **125**, 193 (1980).
[20] H. Hofmann and P. J. Siemens, Nucl. Phys. A **257**, 165 (1976).
[21] A. Iwamoto, K. Harada, S. Yamaji, and S. Yoshida, Z. Phys. A: Hadrons Nucl. **302**, 149 (1981).
[22] H. Ehrenreich and M. H. Cohen, Phys. Rev. **115**, 786 (1959).
[23] J. W. Negele, Rev. Mod. Phys. **54**, 913 (1982).
[24] H. Feldmeier, Rep. Prog. Phys. **50**, 915 (1987).
[25] S. Ayik, K. Washiyama, and D. Lacroix, Phys. Rev. C **79**, 054606 (2009).
[26] G. G. Adamian, R. V. Jolos, A. K. Nasirov, and A. I. Muminov, Phys. Rev. C **56**, 373 (1997).
[27] H. Köhler, Nucl. Phys. A **343**, 315 (1980).
[28] D. Hilscher and H. Rossner, Ann. Phys. (Paris, Fr.) **17**, 471 (1992).
[29] V. Zagrebaev and W. Greiner, J. Phys. G **31**, 825 (2005).
[30] K. Washiyama, D. Lacroix, and S. Ayik, Phys. Rev. C **79**, 024609 (2009).
[31] N. Wang, Z. Li, and X. Wu, Phys. Rev. C **65**, 064608 (2002).
[32] N. Wang, Z. Li, X. Wu, J. Tian, Y. X. Zhang, and M. Liu, Phys. Rev. C **69**, 034608 (2004).
[33] M. Papa, T. Maruyama, and A. Bonasera, Phys. Rev. C **64**, 024612 (2001).
[34] I. Skwira-Chalot *et al.*, Phys. Rev. Lett. **101**, 262701 (2008).
[35] J. Aichelin, Phys. Rep. **202**, 233 (1991).
[36] J. Aichelin and H. Stöcker, Phys. Lett. B **176**, 14 (1986).
[37] E. Wigner, Phys. Rev. **40**, 749 (1932).

[38] C. Hartnack, R. K. Puri, J. Aichelin, J. Konopka, S. Bass, H. Stöcker, and W. Greiner, Eur. Phys. J. A **1**, 151 (1998).
[39] G. Bertsch and S. D. Gupta, Phys. Rep. **160**, 189 (1988).
[40] T. Maruyama, K. Niita, and A. Iwamoto, Phys. Rev. C **53**, 297 (1996).
[41] J. C. Slater, Phys. Rev. **81**, 385 (1951).
[42] T. Maruyama, A. Ohnishi, and H. Horiuchi, Phys. Rev. C **42**, 386 (1990).
[43] J. Tian, X. Li, X. Wu, Z. Li, and S. Yan, Eur. Phys. J. A **42**, 105 (2009).
[44] K. Zhao, Z. Li, X. Wu, and Z. Zhao, Phys. Rev. C **79**, 024614 (2009).
[45] V. N. Kondratyev, A. Bonasera, and A. Iwamoto, Phys. Rev. C **61**, 044613 (2000).
[46] K. Wen, F. Sakata, Z.-X. Li, X.-Z. Wu, Y.-X. Zhang, and S.-G. Zhou, Phys. Rev. Lett. **111**, 012501 (2013).
[47] P. Fröbrich and R. Lipperheide, *Theory of Nuclear Reactions* (Oxford University Press, Oxford, 1996), and references therein.
[48] R. Y. Cusson, P. G. Reinhard, M. R. Strayer, J. A. Maruhn, and W. Greiner, Z. Phys. A: Hadrons Nucl. **320**, 475 (1985).
[49] A. S. Umar, V. E. Oberacker, J. A. Maruhn, and P. G. Reinhard, Phys. Rev. C **80**, 041601 (2009).
[50] R. E. Renfordt, D. Schall, R. Bock, R. Brockmann, J. W. Harris, A. Sandoval, R. Stock, H. Ströbele, D. Bangert, W. Rauch, G. Odyniec, H. G. Pugh, and L. S. Schroeder, Phys. Rev. Lett. **53**, 763 (1984).
[51] V. Denisov and W. Nörenberg, Eur. Phys. J. A **15**, 375 (2002).
[52] M. Brack, C. Guet, and H.-B. Håkansson, Phys. Rep. **123**, 275 (1985).
[53] R. Bass, *Lecture Notes in Physics* (Springer, Berlin, 1980), Vol. 117, p. 281.
[54] K. Washiyama and D. Lacroix, Phys. Rev. C **78**, 024610 (2008).
[55] N. D. Mavlitov, P. Fröbrich, and I. I. Gonchar, Z. Phys. A: Hadrons Nucl. **342**, 195 (1992).
[56] K. Sato, A. Iwamoto, K. Harada, S. Yamaji, and S. Yoshida, Z. Phys. A: Hadrons Nucl. **288**, 383 (1978).
[57] A. K. Dhara, K. Krishan, C. Bhattacharya, and S. Bhattacharya, Phys. Rev. C **57**, 2453 (1998).
[58] N. Loebl, A. S. Umar, J. A. Maruhn, P.-G. Reinhard, P. D. Stevenson, and V. E. Oberacker, Phys. Rev. C **86**, 024608 (2012).